Carbohydrate Polymers 111 (2014) 456–462

Contents lists available at ScienceDirect

Carbohydrate Polymers

journal homepage: www.elsevier.com/locate/carbpol

Enhanced mechanical and thermal properties of regenerated cellulose/graphene composite fibers

Mingwei Tian[a,b,c], Lijun Qu[a,b,c,*], Xiansheng Zhang[a,b], Kun Zhang[d], Shifeng Zhu[a,b], Xiaoqing Guo[a,b], Guangting Han[a,b], Xiaoning Tang[a,b], Yaning Sun[a]

[a] College of Textiles, Qingdao University, Qingdao 266071, Shandong, China
[b] Laboratory of New Fiber Materials and Modern Textile, The Growing Base for State Key Laboratory, Qingdao University, Qingdao 266071, Shandong, China
[c] Collaborative Innovation Center for Marine Biomass Fibers, Materials and Textiles of Shandong Province, Qingdao University, Qingdao 266071, Shandong, China
[d] Department of Industrial Engineering, Texas Tech University, Lubbock, TX 79409, USA

ARTICLE INFO

Article history:
Received 1 March 2014
Received in revised form 18 April 2014
Accepted 8 May 2014
Available online 20 May 2014

Keywords:
Composite fiber
Graphene oxide
Mechanical properties
Thermal analysis
Thermal insulation

ABSTRACT

In this study, a wet spinning method was applied to fabricate regenerated cellulose fibers filled with low graphene loading which was systematically characterized by SEM, TEM, FTIR and XRD techniques. Subsequently, the mechanical and thermal properties of the resulting fibers were investigated. With only 0.2 wt% loading of graphene, a ~50% improvement of tensile strength and 25% enhancement of Young's modulus were obtained and the modified Halpin–Tsai model was built to predict the mechanical properties of composite fibers. Thermal analysis of the composite fibers showed remarkably enhanced thermal stability and dynamic heat transfer performance of graphene-filled cellulose composite fiber, also, the presence of graphene oxide can significantly enhance the thermal conductivity of the composite fiber. This work provided a facile way to improve mechanical and thermal properties of regenerated cellulose fibers. The resultant composite fibers have potential application in thermal insulation and reinforced fibrous materials.

1. Introduction

Graphene is the name given to a flat monolayer of carbon atoms tightly packed into a two-dimensional (2D) honeycomb lattice (Geim & Novoselov, 2007), possesses a number of extraordinary electronic, thermal and mechanical properties (Zhang, Li, & Pan, 2012; Balandin et al., 2008; Pandele et al., 2014), especially, it has been reported that a single-layered graphene was found to exhibit a Young's modulus of ~1100 GPa and tensile strength of 130 GPa. Similar to CNTs, graphene has demonstrated a high carrier mobility of 15,000 $cm^2 V^{-1} s^{-1}$ at room temperature and maintained current densities of six orders of magnitude higher than the copper. Graphene is thermally stable with thermal conductivities of up to 5000 $W m^{-1} K^{-1}$, higher than CNTs and metals such as gold, silver, and copper (Sun et al., 2013).

Compared with carbon nanotube (Sun et al., 2013; Rafiee et al., 2009; Martin-Gallego et al., 2013), graphene is usually recommended as a great candidate to develop multifunctional materials with enhanced properties. One-dimensional macrostructure graphene fiber is a relative novel area with attractive potential applications. The graphene fibers can be generally classified into two categories, the neat graphene fibers and the graphene composite fibers. In the neat graphene fiber issue, for instance Xu and Gao (2011) firstly manufactured pristine graphene fiber by wet-spinning, Dong et al. (2012) also reported a pristine graphene fiber prepared by the process of glass pipeline and Chen et al. (2013) achieved high performance and better understanding on the processing–structure–property relationship of graphene fibers by the wet-spinning and coagulation process. However, the yields of above obtained fibers are limited in the lab—scale level, and their procedures are usually manual, discontinuous and low efficiency. Moving to the graphene composite fibers, spinning methods used to create composite fibers containing graphene include melt-spinning, solution-spinning and electrospinning. Many kinds of polymers have been utilized to prepare the polymer/graphene composite fibers, He et al. (2012) prepared

* Corresponding author at: Corresponding author. Tel.: +86 053285950893; fax: +86 053285953076.
E-mail address: lijunqu@126.com (L. Qu).

http://dx.doi.org/10.1016/j.carbpol.2014.05.016
0144-8617/

sodium alginate/graphene oxide (NaAlg/GO) fibers with enhanced mechanical strength via a lab-scale wet spinning method, Shin et al. (2012) obtained graphene/CNT/PVA nanocomposite fiber, and the strength of the nanocomposite fiber has been greatly improved compared with pristine PVA fiber. Xu and Gao (2010) fabricated PA6 grafted graphene composite fibers revealing an excellent reinforcement to composites by graphene. So far, however, little research has been reported on natural polymers used as the matrix for preparing graphene-containing/polymer composite fibers. Furthermore, some other potential properties of grapheme/polymer fibers, such as thermal properties, were not sufficiently carried on in the previous work.

Cellulose, the most abundant natural polymer in nature, is renewable, biodegradable and biocompatible, and its derivative, regenerated cellulose fibers, comprised of linear polysaccharide exhibited outstanding properties (Li et al., 2010; Zhang et al., 2007; Wang et al., 2013; Jiang et al., 2012), i.e. high moisture absorbency, flexibleness, dyeability, but revealed unfavorable mechanical properties. For instance, the tenacity of regenerated cellulose fibers are usually in the range of 1.8–2.5 cN/dtex which is definitely lower than cotton fiber (~4.5 cN/dtex) and some synthetic fibers, i.e. polyester fiber (~4.7 cN/dtex), polypropylene fiber (~6.5 cN/dtex) (Hearle & Morton, 2008), therefore, the modified regenerated cellulose fibers with reasonable mechanical properties could extend and escalate their potential applications. As far as we know, no studies have carried on the modified regenerated cellulose fiber with low graphene content to improve their mechanical performance and wearability. In this paper, regenerated cellulose/graphene composite fibers were fabricated by a continuous pilot-scale wet spinning procedure and their micro-structure, crystallization behavior, mechanical properties, and thermal properties were characterized and illustrated.

2. Materials and methods

2.1. Preparation of graphene oxide nanoflakes

Graphite powder was expanded to exfoliated graphene based on the modified Brodie's method (Wang et al., 2009). 20 g of graphene powder (nature flake graphite, sized at 30 μm), 260 mL of fuming nitric acid and 160 g of sodium chlorate were mixed and stirred for 24 h using a magnetic stirrer at room temperature. Then the resultant solution was washed 5 times with 200 mL of 5% hydrochloric acid and 7 times with 1 L of distilled water to remove all acidic and saline impurities. Graphite oxide was collected through a precipitation method and evaporation of the solution at 60 °C. 8 mg/mL graphene oxide dispersion (GO) was fabricated with ultrasonication for 30 min and stabilized with assistance of ammonia.

2.2. Preparation of regenerated cellulose/graphene composite fibers

The pilot-scale production route and the apparatus of the spinning process (Speakman & Chamberlain, 1944) are shown in Fig. 1. Regenerated cellulose aqueous solution (α-cellulose 8.2 wt%, NaOH 5.5 wt%) was kindly provided by Shandong Helon Group Co. Ltd., graphene oxide solution 8 mg/mL with different amount (0, 300 mL, 600 mL) were injected into 300 L regenerated cellulose solution, respectively, forming hybrid spinning solutions with different graphene loading: 0%, 0.1 wt% and 0.2 wt%. The resultant spinning solutions were vigorously stirred at room temperature for 6 h to form homogenous solutions in 500 L dissolution tank (a). After filtered by filter papers (b), and degassed in storage tank (c) under diminished pressure and vacuum condition, spinning solutions were quantitatively transferred with flow control pump (d). A

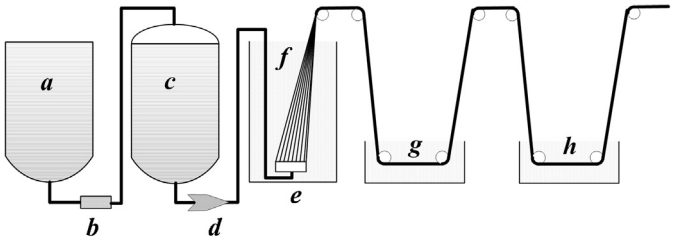

Fig. 1. The pilot-scale production route and the apparatus of the spinning process.

30-hole (0.08 mm diameter) spinneret (e) was employed to extrude the solutions into coagulating bath solution (f) of H_2SO_4 100 g/L, Na_2SO_4 300 g/L, $ZnSO_4$ 15 g/L at 35 °C. The spun fibers were washed and stretched (stretching ratio is 20%) in washing bath (g) with further dehydration in the alcohol leaching bath (h). According to Fan et al. (2008), under strong alkaline solution (NaOH or KOH), exfoliated graphite oxide can be directly reduced and deoxygenated into graphene. Since in our route the hybrid spinning solution was strong alkaline solution (NaOH 5.5 wt%), stable regenerated cellulose/graphene spinning solutions can be facilely prepared in the absence of reducing agents.

Then, a series of composite fibers were prepared as pristine regenerated cellulose fiber, regenerated cellulose/graphene fiber (0.1 wt%), regenerated cellulose/graphene fiber (0.2 wt%) and labeled as RC, RC/G 0.1 and RC/G 0.2, respectively.

2.3. Characterization and measurement

The morphology of the resulting graphene and composite fibers were investigated through SEM (JEOL JSM-840 SEM) and transmission electron microscopy (TEM, JEOL-JEM 2100). Fourier-transform infrared (FT-IR) spectra were recorded on a Nicolet 5700 FT-IR Spectrometer (Thermo Nicolet Corporation, USA) with the wave number range of 500–4000 cm^{-1} (KBr disk). X-ray diffraction (XRD) measurements were performed on a D8 ADVANCE X-ray diffract meter equipped with a Cu *K*a radiation source (λ = 1.5406 Å) operating at 40 kV and 40 mA in the range of 2θ = 5–60°.

Mechanical properties of composite fibers were conducted with FAVIMAT Single Fiber Electronic Tensile Strength Tester (Textechno, USA) according to ASTM D3822, and the work condition was at 20 °C and relative humidity of 65%. The initial gage length was set at 15 mm and the crosshead speed at 10 mm/min and a pretension of 0.02 cN/dtex. All fibers were tested 50 times and their average value was reported.

Thermal behaviors of samples were characterized with a NETZSCH STA 409 PC/PG, using a heating rate of 10 K/min from 25 to 800 °C in a nitrogen atmosphere. Furthermore, the thermophysical properties (thermal conductivity, thermal diffusivity and specific heat capacity) of our fiber assemblies were simultaneously obtained by the transient approach proposed from Tian, Zhu, and Pan (2012a).

2.4. Dynamic heat transfer of composite fiber assemblies

In order to elucidate the enhanced heat transfer of the margin graphene filler in the resulting fibers, we utilized a setup apparatus in our lab to simulate the dynamic thermal response of fiber assemblies under unsteady-state conditions. As shown in Fig. 2, 10 g fiber assemblies were homogeneously laid in a flask and a thermometer was placed at the center of the flask. For each case, the filled flask was moved into a 100 °C water bath from the initial temperature 30 °C, meanwhile, the fixed thermometer measured the temperature curve and then recorded by a computer system at 1 s interval.

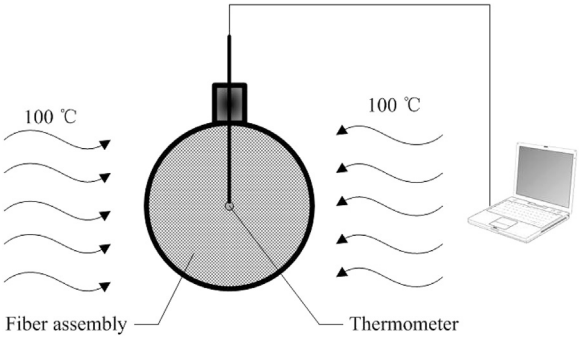

Fig. 2. The schematic diagram of measuring apparatus.

3. Results and discussion

3.1. Structure characterization of graphene oxide

The featured characterization of resultant graphene oxide was investigated as shown in Fig. 3, TEM images of the nanosheets were given in Fig. 3a, the fully exfoliated single-layer graphene could be detected and some graphene nanosheets crumple due to the atomic thickness. UV–vis spectra of the sample was illustrated in Fig. 3b, as depicted in Xu and Gao (2011) and Xu et al. (2013), the curve of graphite oxide dispersion exhibited a maximum peak at 238 nm and tiny shoulder at 302 nm, which were, respectively, attributed to $\pi \rightarrow \pi^*$ transitions of aromatic C—C bonds and $n \rightarrow \pi^*$ transitions of C=O bonds. In FTIR studies of GO in Fig. 3c, characterization peaks appearing at 1725 cm^{-1}, 1627 cm^{-1}, 1405 cm^{-1}, 1218 cm^{-1} and 1050 cm^{-1} were attributed to C=O, O—H vibrations, O—H deformation vibration, epoxy rings and C—OH bending, respectively, which was similar with Mathesh et al. (2013). In addition, the XRD patterns of graphite and GO were shown in Fig. 3d. The characteristic peak at 26.5° corresponds to the (0 0 2) diffraction with the *d*-spacing of ~0.34 nm, for the XRD pattern of GO, the characteristic diffraction peak appeared to be 8.9°, corresponding to the layer-to-layer distance of ~0.78 nm indicating the successful oxidation of graphite (Luo et al., 2012).

3.2. Morphology and structure of composite fibers

Photograph, SEM and TEM images were employed to reveal the morphology of composite fibers. The RC/G 0.1 and RC/G 0.2 fibers expressed sliver and dark gray resulting from the incorporation of graphene fillers (see Fig. 4a). The SEM images of fracture-section of our samples were illustrated in Fig. 4b–d. Apparently, all the fibers had relatively uniform diameters (15–20 μm) and their corresponding fracture-section appeared to have some irregular striations, which could be caused by the coagulation of viscose solution that took place first on the surface and then further delayed coagulation in the interior during the spinning process. The RC fiber showed a smooth fracture surface morphology (Fig. 4b). For RC/G 0.1 and 0.2 fibers, their fracture surface became relatively crude, which indicated that more energy was required to break the composites and graphene oxide formed strong interface with cellulose molecule chains. In addition, the fracture surface of RC/G 0.1 and 0.2 fibers did not show definitely GO aggregations demonstrating that the homogenous composite structures were stably formed. Moreover, the homogenous dispersion between graphene oxide and its matrix of RC/G 0.2 could also be clearly detected in TEM (Fig. 4e), the homogenous dispersion of graphene could also predict the enhancement of the tensile strength.

The FTIR spectra of fibers were shown in Fig. 5. In RC fiber, absorption peaks at 3410, 2930, 1640, 1400 and 1050 cm^{-1} were attributed to the OH stretching, CH stretching, OH of water

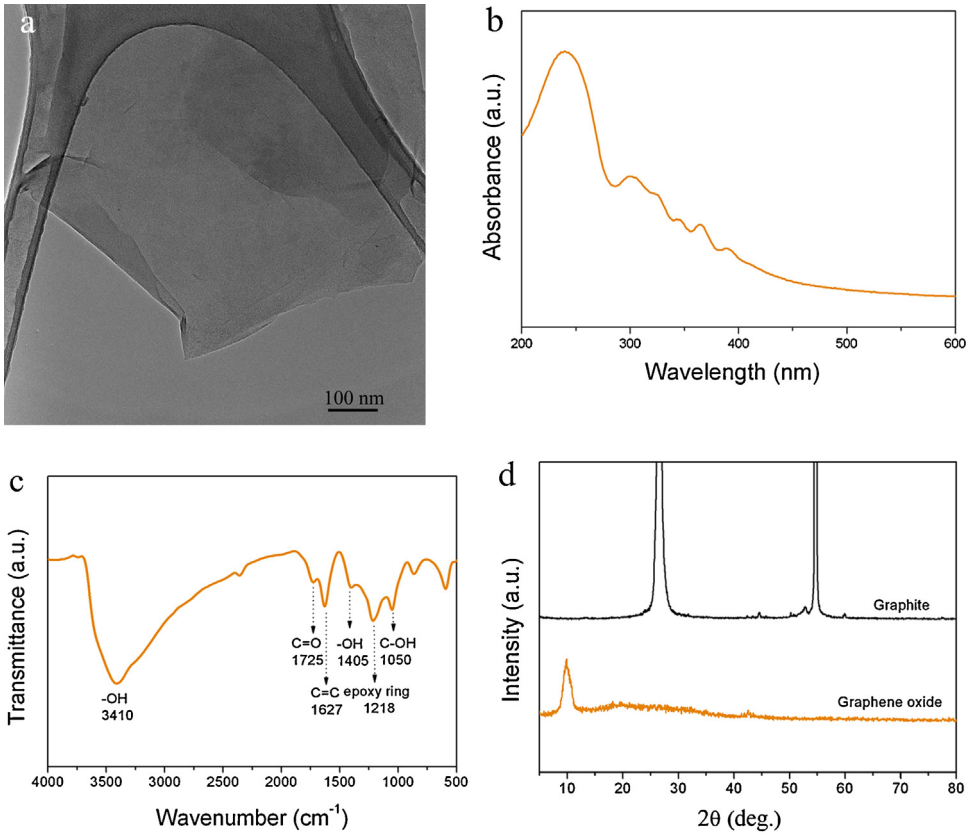

Fig. 3. UV–vis absorption spectrum of graphene oxide (a). TGA curves (b), FT-IR (c) and XRD pattern (d).

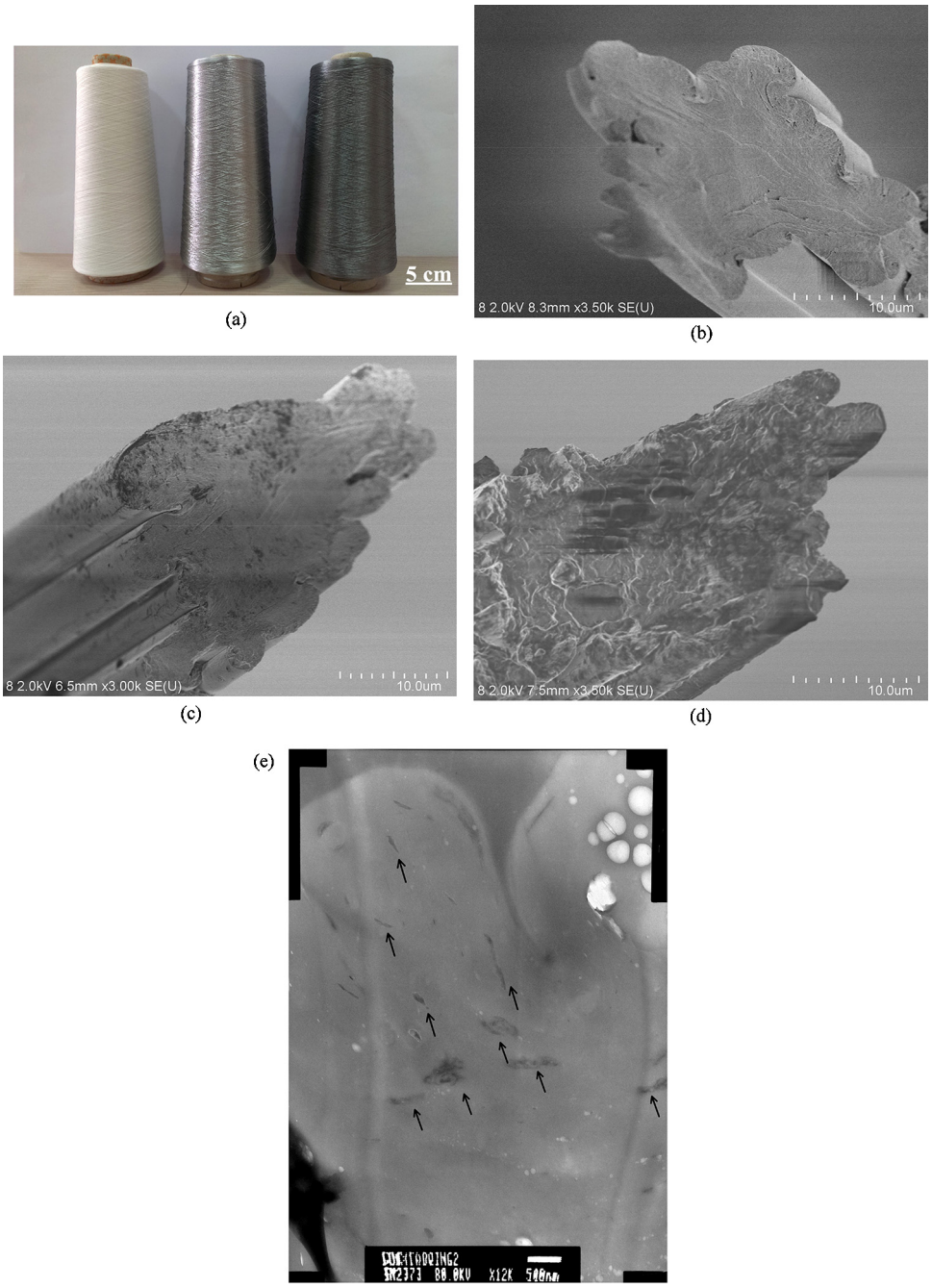

Fig. 4. The morphologies of composite fibers, photograph of the composite fibers (a), SEM of the cross-section of RC fiber (b), RC/G 0.1 fiber (c), RC/G 0.2 fiber (d) and TEM of RC/G 0.2 fiber (e).

absorbed from cellulose, CH_2 symmetric bending and C—O stretching, respectively (Carrillo et al., 2004). In RC/G 0.1 and RC/G 0.2 fibers, with the increasing graphene content, several absorption bands of composite fibers were gradually changed as follow, the characteristic peaks at 3410 cm^{-1} and 1640 cm^{-1} shifted to higher and sharper, ascribing to the combined influence of the added graphene. These peaks were assigned to OH and C=C stretching of the benzenoid rings of graphene, respectively (Jin et al., 2013).

Fig. 6 shows XRD patterns of composite fibers, the RC fiber shows three peaks at $2\theta = 12.4$, 20.2, and 22.2°, which are assigned to the (1 1 0), (1 $\bar{1}$ 0), and (2 0 0) planes of crystalline cellulose II (Li et al., 2010). The diffraction angles of the composite fibers were similar to the pure RC fiber. With the increasing graphene contents, the stronger diffraction intensity of the RC/G fibers in comparison to that of RC fiber at the above three peaks indicated a slightly higher crystalline degree, Thus we can conclude that the crystalline degree of regenerated cellulose fiber increased after adding graphene filler.

3.3. Mechanical properties and prediction model

Tensile properties of graphene composite fibers and the neat RC fiber were shown in Fig. 7. Obviously, the addition of graphene reinforced the ultimate tensile strength (see Fig. 7a). The tensile strength of the RC/G 0.2 fiber was ~360 MPa, which is about 50% larger than the neat RC fibers (~240 MPa). Remarkably, this improvement was achieved at a very low graphene loading (0.1–0.2 wt%). Fig. 6b shows the Young's module of cellulose fibers. Incorporation of 0.1 wt% and 0.2 wt% graphene increased

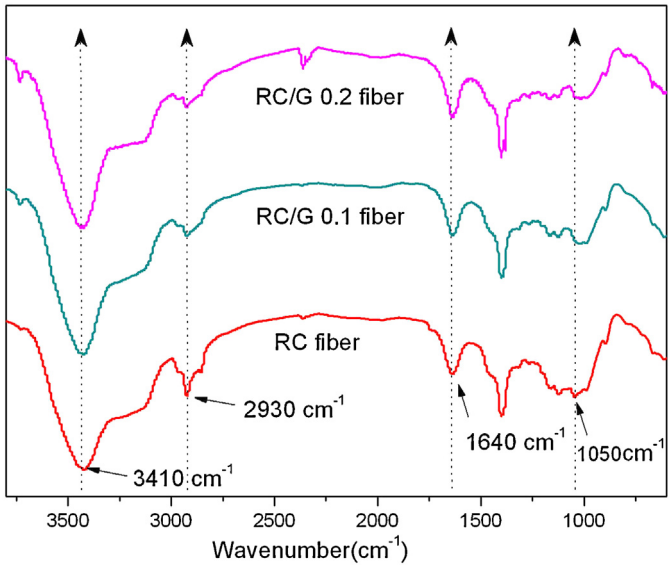

Fig. 5. FTIR spectrum of the composite fibers.

the Young's Modulus from ~1.25 to ~1.34 GPa for RC/G 0.1 while 25% improvement for RC/G 0.2 in comparison to that of neat fibers. The increment of tensile strength should be attributed to the good coherence between the regenerated cellulose matrix and graphene fillers, and the presence of strong interactions, which was confirmed by FTIR and XRD patterns.

In order to theoretically investigate the tensile properties, a modified Halpin–Tsai model for graphene composite fiber derived (Rafiee et al., 2009) was employed to predict the Young's modulus of our obtained graphene composite fibers and the corrected equation as follow,

$$E_C = \frac{3}{8}\frac{1+\xi\eta_L V_G}{1-\eta_L V_G} \times E_M + \frac{5}{8}\frac{1+2\eta_W V_G}{1-\eta_W V_G} \times E_M \quad (1)$$

$$\eta_L = \frac{(E_G/E_M)-1}{(E_G/E_M)+\xi} \qquad \eta_W = \frac{(E_G/E_M)-1}{(E_G/E_M)+2} \quad (2)$$

where E_C is the composite elastic modulus, V_G moreover, the miscibility between graphene and its matrix of RC/G 0.2 was clearly

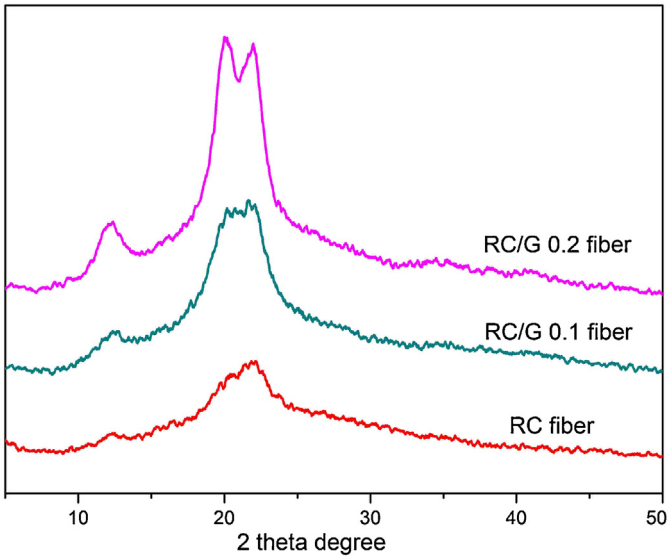

Fig. 6. XRD spectrum of the composite fibers.

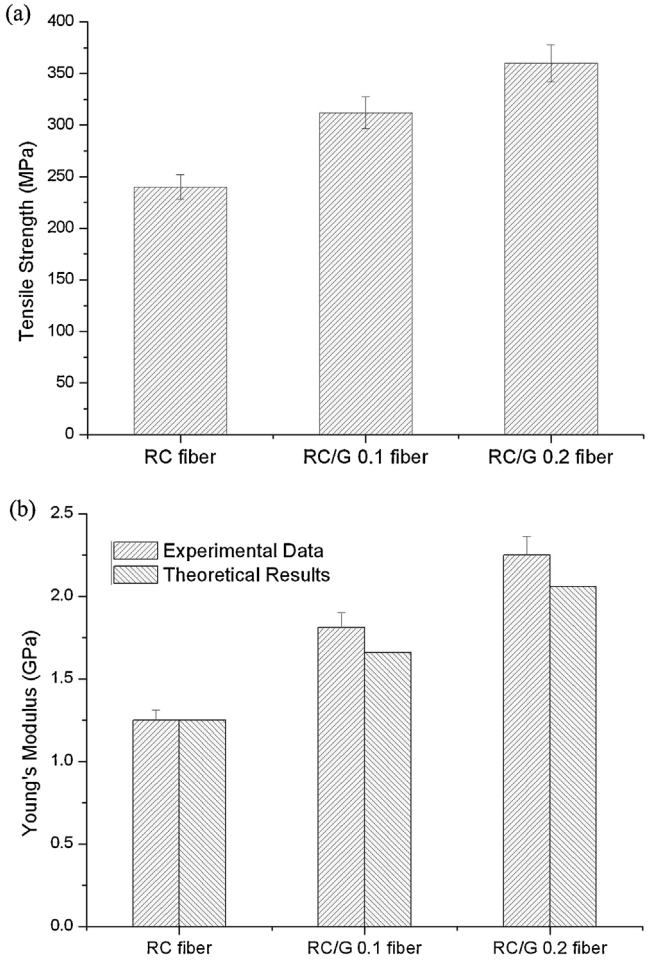

Fig. 7. The mechanical properties of the composite fibers, tensile strength (a) and Young's modulus (b).

detected in TEM (Fig. 4e), the homogenous dispersion of graphene could also predict the enhancement of the tensile strength is the volume fraction of the inserted graphene, E_G and E_M are the effective graphene (~1.01 TPa) and matrix modulus (here, regenerated cellulose matrix ~1.25 GPa), respectively. The parameter ξ depends on the geometry and boundary conditions of graphene, which can be expressed by

$$\xi = 2\frac{(W+L)/2}{t}$$

where W, L and t represent the average graphene width (1.5 μm), length (2.5 μm) and thickness (1.5 nm), respectively, another parameter V_G can be calculated as, $V_G = \frac{W_G}{W_G+(\rho_G/\rho_M)(1-W_G)}$ where W_G is the weight fraction of graphene (0.1% and 0.2%), ρ_G and ρ_M are the density of graphene (ρ_G = 1.06 g/cm^3) and rengerated cellulose (ρ_M = 1.5 g/cm^3), respectively.

The theoretical predictions of the resultant fibers were calculated based on Eqs. (1) and (2) and compared with our experimental results in Fig. 7b. theoretical Young's modules of RC/G 0.1 and 0.2 fibers were both ~8% lower than the experimental results which might be caused by the wrinkled structure of actual graphene compared with the smooth flat rectangular shape assumed in the prediction model. Therefore, this model can be proposed as a facile route to predict the Young's Modulus of the graphene composite fibers with various polymer matrixes.

Table 1
TGA values for neat RC fiber and its composite fibers.

Sample	Onset (°C)	Endset (°C)	T (°C) for 10% loss	T (°C) for 50% loss	Char (%)
Neat RC fiber	265	341	292 ± 2.0	330 ± 2.0	16 ± 3.5
RC/G 0.1 fiber	298	358	301 ± 2.5	336 ± 2.5	19 ± 4.5
RC/G 0.2 fiber	309	377	313 ± 1.5	355 ± 1.5	20 ± 4.0

Table 2
Thermal conductivity, thermal diffusivity, volumetric capacity of composite fibers.

Sample	Thermal conductivity $k \times 10^{-2}$ W m^{-1} K^{-1}	Thermal diffusivity $a \times 10^{-7}$ m^2 s^{-1}	Volumetric capacity $\rho C_p \times 10^5$ J m^{-3} K^{-1}
Neat RC fiber	6.20 ± 0.15	1.32 ± 0.11	4.70 ± 0.10
RC/G 0.1 fiber	7.20 ± 0.11	1.83 ± 0.09	3.93 ± 0.12
RC/G 0.2 fiber	8.15 ± 0.13	2.49 ± 0.13	3.27 ± 0.08

3.4. Thermal properties of the composite fibers

Thermal properties of the composite fibers were elucidated here by the thermal stability (TGA) and dynamic heat transfer. The TGA curves of neat RC fiber and its composite fibers are shown in Fig. 8. It is observed that the neat fibers and the composite fibers showed thermal degradation and significant weight loss with temperature. Furthermore, the onset and the end set of thermal degradation temperature were determined from the intersection of two tangents, and the corresponding TGA analytical values of samples (onset, endset, decomposition temperatures at 10% and 50% weight loss, char content) were given in Table 1. The onset temperature of neat RC fiber was 265 °C, while for the composite fibers it increased to 298 °C for RC/G 0.1 fiber and 309 °C for RC/G 0.2 fiber, and the incorporation of 0.1 wt% and 0.2 wt% graphene in neat regenerated cellulose increased the 50% decomposition temperature by 6 °C and 25 °C, respectively. All the results indicated that the thermal stability of the neat fibers was enhanced by the low graphene filler.

The thermophysical properties of each sample were listed in Table 2. Graphene was reported to have a remarkable high thermal conductivity of 5000 W m^{-1} K^{-1} (Prasher, 2010). As expected, the presence of graphene oxide can significantly enhance the thermal conductivity of RC fiber, a loading of 0.2 wt% graphene oxide (RC/G 0.2 fiber) resulted in a thermal conductivity 8.15 × 10^{-2} W m^{-1} K^{-1}, about 30% improvement on that of neat RC fiber (6.20 × 10^{-2} W m^{-1} K^{-1}). Furthermore, RC/G 0.2 fiber possessed the highest thermal diffusivity value (2.49 × 10^{-7} m^2 s^{-1}), 89% higher than that of RC fiber, but produced the lowest volumetric capacity value (3.27 × 10^5 J m^{-3} K^{-1}), 30% lower than that of RC fiber. All these values implied that the RC/G 0.2 fiber could release quick temperature response under unsteady-state conditions.

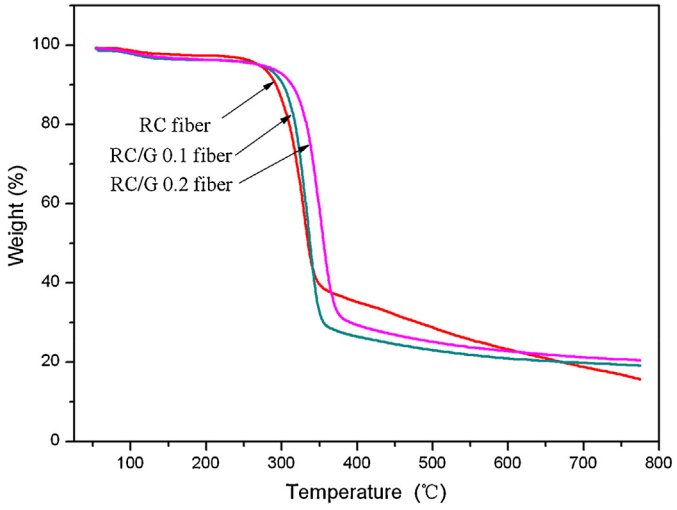

Fig. 8. TGA curves of the composite fibers.

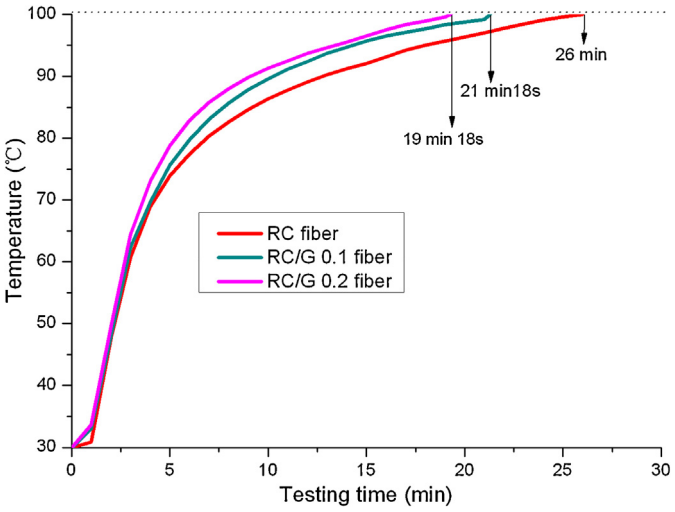

Fig. 9. Dynamic temperature curves of the composite fibers.

In order to verify the above prediction of our composite fibers, the temperature curves of samples along with testing time recorded in our setup apparatus (see Fig. 2) was shown in Fig. 9. Compared three temperature curves, the flask filled with RC/G 0.2 fibers always kept at the highest temperature raising speed through the entire heating process, and the neat fiber assembly expressed the most dilatory temperature response. In consequence, the shortest time (19 min 18 s) was cost for RC/G 0.2 fibers to achieve the destination 100 °C, while RC/G 0.1 fibers was 21 min 18 s and the neat RC fibers exhausted the longest time 26 min. These three dynamic curves verified the prediction that the RC/G 0.2 fiber could release quick temperature response under unsteady-state conditions.

We can employ thermophysical properties of each sample (listed in Table 2) to elucidate this prediction. Dynamic heat transfer process was combined determined by three thermophysical parameters (Tian et al., 2012b,c), thermal conductivity, thermal diffusivity and volumetric capacity, the highest thermal conductivity of the RC/G 0.2 fiber demonstrated it can absorb the most amount of heat from surrounding conditions, and also the lowest volumetric capacity consumed the smallest heat for temperature rising. Therefore, the composite fiber filled with graphene oxide expressed the higher temperature rising curves as plotted in Fig. 9.

4. Conclusion

Regenerated cellulose/graphene composite fibers were continuously prepared by a pilot-scale wet spinning route. Afterwards, it has been proved by mechanical property testing that the addition

of graphene oxide can greatly increase the tensile strength of composite fiber. As a representative example, a 50% increase of tensile strength was achieved by adding 0.2 wt% graphene oxide, indicating the efficient load transfer between the graphene oxide nanosheet and the matrix. The modified Halpin–Tsai prediction model of Young's modulus was verified as an effective model to predict diversity graphene/polymer composite. In addition, the composite fibers also exhibited ideal thermal stability and dynamic heat transfer under high temperature conditions. The incorporation of 0.2 wt% graphene in neat regenerated cellulose increased the onset decomposition temperature by 44 °C. The composite fiber incorporated with graphene oxide could remarkable absorb more heat from surrounding conditions and consume smaller heat for temperature rising. In a word, our prepared composite fibers may be a promising fibrous material with excellent mechanical and thermal insulation properties.

Acknowledgments

This work is supported by National Natural Science Foundation of China (no. 51273097 and 51306095), and Taishan Scholars Construction Engineering of Shandong Province and program for scientific research innovation team in colleges and universities of Shandong province.

References

Geim, A. K., & Novoselov, K. S. (2007). The rise of graphene. *Nature Materials*, *6*(3), 183–191.
Zhang, S., Li, Y., & Pan, N. (2012). Graphene based supercapacitor fabricated by vacuum filtration deposition. *Journal of Power Sources*, *206*(0), 476–482.
Zhang, K., et al. (2010). Graphene/polyaniline nanofiber composites as supercapacitor electrodes. *Chemistry of Materials*, *22*(4), 1392–1401.
Balandin, A. A., et al. (2008). Superior thermal conductivity of single-layer graphene. *Nano Letters*, *8*(3), 902–907.
Pandele, A. M., et al. (2014). Synthesis, characterization, and *in vitro* studies of graphene oxide/chitosan-polyvinyl alcohol films. *Carbohydrate Polymers*, *102*, 813–820.
Sun, X., et al. (2013). Developing polymer composite materials: Carbon nanotubes or graphene? *Advanced Materials*, *25*(37), 5153–5176.
Rafiee, M. A., et al. (2009). Enhanced mechanical properties of nanocomposites at low graphene content. *ACS Nano*, *3*(12), 3884–3890.
Martin-Gallego, M., et al. (2013). Comparison of filler percolation and mechanical properties in graphene and carbon nanotubes filled epoxy nanocomposites. *European Polymer Journal* (in press).
Xu, Z., & Gao, C. (2011). Graphene chiral liquid crystals and macroscopic assembled fibres. *Nature Communications*, *2*, 571.
Dong, Z., et al. (2012). Facile fabrication of light: Flexible and multifunctional graphene fibers. *Advanced Materials*, *24*(14), 1856–1861.
Chen, L., et al. (2013). Toward high performance graphene fibers. *Nanoscale*, *5*(13), 5809–5815.
He, Y., et al. (2012). Alginate/graphene oxide fibers with enhanced mechanical strength prepared by wet spinning. *Carbohydrate Polymers*, *88*(3), 1100–1108.
Shin, M. K., et al. (2012). Synergistic toughening of composite fibres by self-alignment of reduced graphene oxide and carbon nanotubes. *Nature Communications*, *3*, 650.
Xu, Z., & Gao, C. (2010). In situ polymerization approach to graphene-reinforced nylon-6 composites. *Macromolecules*, *43*(16), 6716–6723.
Li, R., et al. (2010). Primarily industrialized trial of novel fibers spun from cellulose dope in NaOH/Urea aqueous solution. *Industrial & Engineering Chemistry Research*, *49*(22), 11380–11384.
Zhang, H., et al. (2007). Regenerated-cellulose/multiwalled-carbon-nanotube composite fibers with enhanced mechanical properties prepared with the ionic liquid 1-allyl-3-methylimidazolium chloride. *Advanced Materials*, *19*(5), 698–704.
Wang, W., et al. (2013). Structure and properties of novel regenerated cellulose fibers prepared in NaOH complex solution. *Carbohydrate Polymers*, *98*(1), 1031–1038.
Jiang, G., et al. (2012). Structure and properties of regenerated cellulose fibers from different technology processes. *Carbohydrate Polymers*, *87*(3).
Hearle, J. W. S., & Morton, W. E. (2008). *Physical properties of textile fibres*. Cambridge, England: Elsevier.
Wang, S., et al. (2009). Thermal expansion of graphene composites. *Macromolecules*, *42*(14), 5251–5255.
Speakman, J. B., & Chamberlain, N. H. (1944). The production of rayon from alginic acid. *Journal of the Society of Dyers and Colourists*, *60*(10), 264–272.
Fan, X., et al. (2008). Deoxygenation of exfoliated graphite oxide under alkaline conditions: A green route to graphene preparation. *Advanced Materials*, *20*(23), 4490–4493.
Tian, M., Zhu, S., & Pan, N. (2012). Measuring the thermophysical properties of porous fibrous materials with a new unsteady-state method. *Journal of Thermal Analysis and Calorimetry*, *107*(1), 395–405.
Xu, Z., et al. (2013). Ultrastrong fibers assembled from giant graphene oxide sheets. *Advanced Materials*, *25*(2), 188–193.
Mathesh, M., et al. (2013). Facile synthesis of graphene oxide hybrids bridged by copper ions for increased conductivity. *Journal of Materials Chemistry C*, *1*(18), 3084–3090.
Luo, Y.-B., et al. (2012). Substrateless graphene fiber: A sorbent for solid-phase microextraction. *Journal of Chromatography A*, *1268*(0), 9–15.
Carrillo, F., et al. (2004). Structural FTIR analysis and thermal characterisation of lyocell and viscose-type fibres. *European Polymer Journal*, *40*(9), 2229–2234.
Jin, Y., et al. (2013). Preparation of stable aqueous dispersion of graphene nanosheets and their electrochemical capacitive properties. *Applied Surface Science*, *264*(0), 787–793.
Prasher, R. (2010). Graphene spreads the heat. *Science*, *328*(5975), 185–186.
Tian, M., et al. (2012b). Effects of layer stacking sequence on temperature response of multi-layer composite materials under dynamic conditions. *Applied Thermal Engineering*, *33*, 219–226.
Tian, M., et al. (2012c). Effects of layering sequence on thermal response of multilayer fibrous materials: Unsteady-state cases. *Experimental Thermal and Fluid Science*, *41*, 143–148.